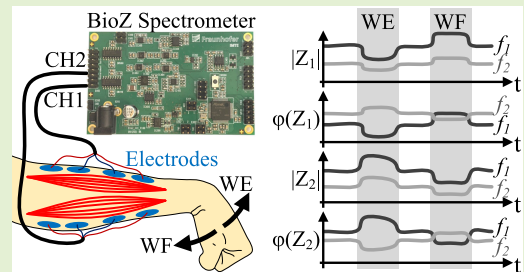


# A Wearable Dual-Channel Bioimpedance Spectrometer for Real-Time Muscle Contraction Detection

Roman Kusche<sup>ID</sup>, Member, IEEE, Andra Oltmann<sup>ID</sup>, and Philipp Rostalski<sup>ID</sup>, Member, IEEE

**Abstract**—The reliable detection of muscle contractions in real-time is important for many applications. Both for prosthesis control and in the field of human-computer interaction, the physiological commands of the user must be recognized. However, conventional methods such as electromyography (EMG) are susceptible to interferences. A particularly robust method is the electrical impedance myography (EIM). Especially the temporal changes of the bioimpedance phase response are of interest for muscle activity monitoring. However, available wearable measurement systems are not capable of detecting muscle contractions in real-time to control prostheses or human-computer interaction devices. This work presents the development and metrological characterization of a wearable real-time bioimpedance spectrometer for the detection of muscle contractions. It can record the frequency responses in the range of 20–230 kHz from two antagonistic muscles. The sampling rate of 25 impedance spectra per second and per channel provides sufficient temporal resolution for many applications. Phantom measurements show that the statistical errors are below 1% for the magnitude and below 0.4° for the phases, which is sufficient for EIM. This system is used to perform first subject measurements. For the first time, these measurements demonstrate the temporal impedance behavior and frequency responses of two antagonistic muscles during contraction. In addition, the directional dependence of the EIM during a muscle contraction is investigated for the first time. The presented measurement system and novel measurement approaches are promising for many EIM applications, especially for reliable muscle contraction detection e.g. in prosthetics or human-computer interaction applications.

**Index Terms**—Bioelectrical impedance, electrical impedance myography (EIM), human-computer interaction, human-machine interface, instrumentation, measurement system, muscle contractions, prosthesis control, real-time, wearable.



Manuscript received 4 January 2024; accepted 24 January 2024. Date of publication 2 February 2024; date of current version 2 April 2024. This work was supported in part by the European Union—European Regional Development Fund and in part by the Federal Government and Land Schleswig-Holstein through the Project “Diagnose- und Therapieverfahren für die Individualisierte Medizintechnik (IMTE)” under Project 12420002. The associate editor coordinating the review of this article and approving it for publication was Prof. Maryam Shojaei Baghini. (Corresponding author: Roman Kusche.)

This work involved human subjects or animals in its research. Approval of all ethical and experimental procedures and protocols was granted by the Institutional Ethics Committee of the University of Lübeck under Application No. 21-020.

Roman Kusche is with the Fraunhofer Research Institution for Individualized and Cell-Based Medical Engineering (IMTE), 23562 Lübeck, Germany, and also with the Department of Computer Science, Hamburg University of Applied Sciences, 20099 Hamburg, Germany (e-mail: roman.kusche@haw-hamburg.de).

Andra Oltmann is with the Fraunhofer Research Institution for Individualized and Cell-Based Medical Engineering (IMTE), 23562 Lübeck, Germany.

Philipp Rostalski is with the Fraunhofer Research Institution for Individualized and Cell-Based Medical Engineering (IMTE), 23562 Lübeck, Germany, and also with the Institute for Electrical Engineering in Medicine, Universität zu Lübeck, 23562 Lübeck, Germany.

Digital Object Identifier 10.1109/JSEN.2024.3359284

## I. INTRODUCTION

**D**URING the past few years several technical applications have been developed in which the detection of muscle contractions has been utilized. The acquired and decoded information can be used to send commands to a computer or to control prostheses intuitively [1], [2], [3], [4]. Very often, the surface electromyography (EMG) is used to measure muscle contractions. This method is based on the noninvasive acquisition of the electrical potentials that occur within a muscle during contraction [5], [6], [7]. For that, commercially available electrodes are placed onto the skin above the muscle or muscle group of interest. A simple electronic measurement circuit amplifies, filters, and typically digitizes the voltage signals [8], [9], [10], [11]. Although the EMG is well-known and widely used, it has some disadvantages. One drawback is that the EMG is a passive method and therefore depends on the energy generated by the human body. It can therefore only detect movements that were caused by active muscle contractions. Other causes of muscle contractions or relaxations such as the sliding down of an arm from the

table cannot be detected. A second challenging point is the stochastic behavior of the EMG signal in a frequency range between 20, . . . , 200 Hz [12], [13]. Typical motion artifacts are in a very similar frequency range, which makes it difficult to differentiate between actual muscle contractions and disturbances [14], [15].

In the past, it has been shown that also the passive electrical properties of the tissue change during contraction [16], [17], [18]. The corresponding promising measurement technique is electrical impedance myography (EIM). It uses a similar electrode configuration like the EMG but requires a significantly more complex measurement circuitry. However, the advantage is that EIM can be more reliable than EMG under certain conditions and can provide additional information [18], [19], [20]. For example, it has been shown that contracting muscles cause very specific changes in the phase response. In contrast to mechanical disturbances, actual muscle contractions cause more negative phases at low frequencies and more positive phases at higher frequencies [21]. This information could be useful for controlling prostheses and requires a simultaneous acquisition of the complex bioimpedance in a wide frequency range. Since the EIM is an active measurement with a defined excitation, the useful signals can be distinguished from statistical errors, in contrast to EMG setups [18].

To determine the electrical tissue properties, small known alternating currents of a few milliamperes in the frequency range from approximately 10 to 500 kHz are applied to the tissue and the resulting voltage drop across the corresponding tissue section is measured. The electrical impedance can then be calculated from the relationship between current and voltage [22], [23], [24]. A well-known application of this one-time measurement is the determination of the human body composition often implemented in scales, like BF511 (OMRON, Mannheim, DE) or the mBCA series (seca, Hamburg, DE) [25], [26]. If the electrical bioimpedance is recorded as a function of time, further applications can be realized. Popular applications in research are impedance cardiography to approximate cardiac output or detection of arterial pulse waves to estimate arterial stiffness [24], [27], [28], [29], [30]. In addition, there is preliminary work that focuses on EIM as a function of time so that the timing of muscle contractions can be detected. However, these works are either limited to single-frequency measurements or provide just one measurement channel [18], [19], [20], [21], [31]. However, in order to take advantage of the EIM, several measurement channels are required, which do not only measure at one frequency, but determine the complex impedance spectra as a function of frequency. In order to use this information for controlling computers, prostheses or other actuators these signals must be acquired and evaluated in real-time [32]. Therefore, the aim of this work is the development of a wearable real-time bioimpedance measurement system for spectral EIM. In this context, wearable means that the system can be battery-operated. It must also have small dimensions and low weight, which do not discomfort the user.

In order to examine the behavior of the contracting muscle and the stretched muscle simultaneously, a dual-channel system is required.

TABLE I  
OVERVIEW OF WEARABLE BIOIMPEDANCE SYSTEMS

System	Freq. Range	Complex	Channels	$f_{s,Spec.}$
Dheman 2021 [33]	10-100 kHz	yes	1	20 Hz
Usman 2022 [34]	50 kHz	yes	1	-
Qiu 2022 [35]	96 kHz	no	1	-
Critcher 2022 [36]	1-128 kHz	yes	4 (MUX)	$\sim 3$ Hz
Mabrouk 2020 [37]	5-100 kHz	yes	1	0.05 Hz
Jung 2021 [38]	50 kHz	no	1	-
Ngo 2022 [19]	2-200 kHz	no	1	n/a
Ferreira 2017 [26]	5-270 kHz	yes	1	n/a

An overview of recently published relevant wearable bioimpedance systems is given in Table I. It can be seen that most systems provide just one bioimpedance channel. Only the system by Critcher et al. [36] is capable of acquiring up to four channels via multiplexing. However, the system's sampling rate ( $f_{s,Spec.}$ ) of approximately three complex spectra per second is too low to detect fast muscle contractions. Furthermore, the frequency range limits the usage for reliable muscle contraction detection, as described in Section II-B.1.

In Section II-A, we first focus on the basics of bioimpedance spectroscopy and EIM. Then, the technical implementation of the system is introduced and its technical capabilities are characterized. Afterward, first subject measurements are presented to demonstrate the functionality of the system under realistic conditions and to propose new measurement approaches.

The main contributions of this work are as follows.

- 1) The development of a wearable dual-channel bioimpedance spectrometer.
- 2) The realization of a real-time interface for training or prosthesis control.
- 3) The first simultaneous measurement of the impedance spectra of two counteractive muscles.
- 4) The first time-resolved measurement of the direction dependency of the complex bioimpedance spectra during muscle contraction.

The results of this work focus particularly on prosthetic control, but can also be easily applied to human-computer-interaction applications.

## II. MATERIALS AND METHODS

### A. Electrical Impedance Myography

Bioimpedance measurement is a well-known method to determine the electrical conductivity of tissue. The results are affected by the composition of different tissue structures with different conductivities. For example, the intracellular and extracellular fluids illustrated in Fig. 1(a) are rather good electrical conductors. The cell membranes, on the other hand, have a more insulating character [22]. The resulting multiple transitions between conductors and insulators lead to a capacitive impedance component in addition to a resistive behavior. This characteristic behavior is often described in the literature by a simplified equivalent circuit according to Fig. 1(b) [39], [40], [41], [42].

Since the conductivity of an electrical capacitance depends on the signal frequency, the total bioimpedance also has

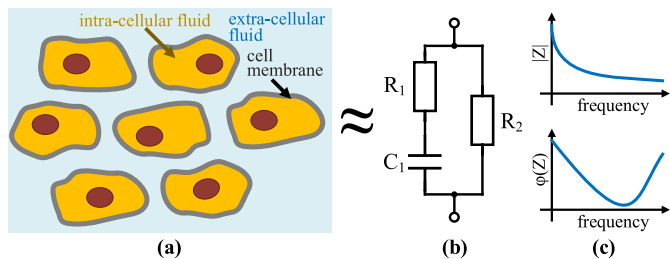


Fig. 1. Illustration of the relationship between the tissue and the frequency-dependent complex bioimpedance. In (a) an exemplary arrangement of cells is illustrated. Its simplified passive electrical behavior can be modeled as an equivalent circuit, as shown in (b) leading to the typical frequency response, depicted in (c).

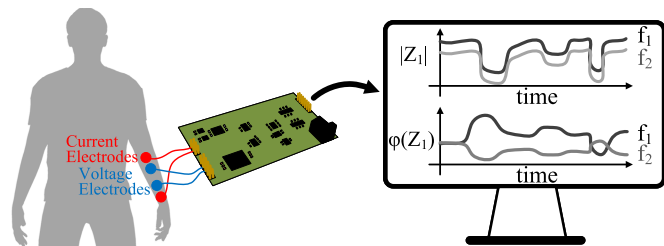


Fig. 2. Typical measurement setup to acquire muscle activity via electrical impedance myography. The excitation current is applied via the outer electrodes (red) and the occurring voltage drop is measured via the inner electrodes (blue). The signals are then processed via the measurement system and displayed.

an individual frequency behavior. An exemplary frequency response of such an RCR element and thus that of a bioimpedance is shown in Fig. 1(c). Since the geometric tissue properties of a measured area change significantly with the contraction of a muscle, the complex frequency-dependent bioimpedance also varies. These changes correspond to the desired signal in this work.

To measure the bioimpedance, four surface electrodes are placed onto the skin as shown in Fig. 2. The measuring system then applies an alternating current into the tissue via the outer two electrodes (red). Simultaneously, the resulting voltage drop is derived from the two inner electrodes (blue). The measuring system either evaluates the bioimpedance by means of analog electronics or first digitizes the current and voltage signals. These are then further processed by the digital part of the measuring system or by a connected PC.

If the frequency response of the bioimpedance is to be determined, the procedure is either repeated using different signal frequencies or simultaneous multifrequency excitation is used [24]. Since this work focuses on transient multifrequency measurement for real-time applications, the final goal is to directly output the bioimpedance signals to a monitor.

A promising feature of impedance myography is the characteristic frequency response [21], [43]. This information can be used, for example, to ensure that an actual muscle contraction has occurred and that the bioimpedance has not just been affected by motion artifacts. Fig. 3 shows a typical hand movement (a) and the resulting changes in the frequency response (b), measured at the underside of the forearm. It can be seen that the impedance magnitude  $|Z|$  decreases for

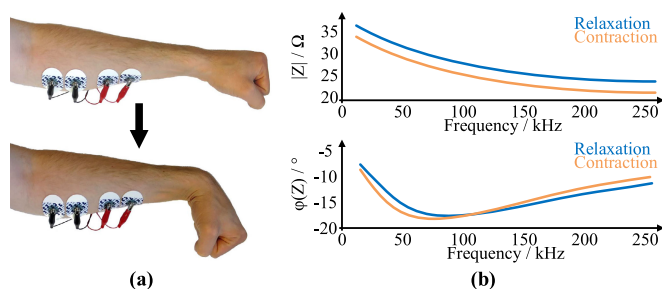


Fig. 3. Representation of the frequency response (b) during a muscle contraction (a). It can be seen that the whole magnitude response decreases during the contraction. In contrast, the change in the phase response has a significant frequency dependency.

an almost constant value over the entire shown frequency range. However, the phase response has a specific characteristic. The measured phase becomes more negative in the low-frequency range and more positive in the higher frequency range. Previous measurements have shown that the intersection of the two-phase responses is approximately between 50 and 150 kHz [21].

## B. System Design

1) *Requirements*: To achieve the desired functionality, the system must fulfill certain technical requirements. First, it must be a dual-channel system with synchronized impedance acquisition. According to the preliminary studies, these channels must be capable to measure complex bioimpedances in the frequency range from 50 to 150 kHz [21], [44]. For an acceptable user or patient interaction feedback, the system has to be capable of measuring at least ten complex frequency responses per second and per channel [32]. Since rather the transient changes than the absolute values of the bioimpedances are useful to detect muscle contractions, the systematic measurement errors are not relevant for this EIM application [18]. For potential use in other sensing applications, such as body composition studies, errors below 5% or below  $2^\circ$  are accepted in this work. For the detection of muscle contractions, the measurement uncertainties are more critical. According to the plot in Fig. 2 and further preliminary work, changes of  $|\Delta Z| = 10\%$  or  $|\Delta\phi| = 1^\circ$  occur during a muscle contraction [18], [21]. In order to be able to not only detect the contraction but also to quantify it, the measurement uncertainties should be lower. In addition, most realistic applications require the system to be mobile. The necessary computing power and energy supply should therefore be feasible to be wearable.

2) *Concept*: To fulfill these requirements, a new measurement system was developed. Most mobile applications require a battery lifetime of several hours. To be able to use conventional smartphone batteries for the power supply, the power consumption of the system should be below approximately 5 W. This can be realized by means of sufficiently powerful but energy-saving microprocessors or controllers. As shown in Fig. 4, the system has a modular design. It consists of a bioimpedance analog front-end (BioZ-AFE), a communication interface (COM\_IF), and an evaluation and display unit. In order to meet the special requirements, the BioZ-AFE is

newly developed printed circuit board (PCB). For the realization of the COM\_IF, a commercially available microcontroller board (Teensy 4.1, PJRC.COM, LLC., Sherwood, OR, USA) with integrated analog-to-digital converters (ADCs,  $f_s = 650$  kHz, 12 bits) is chosen. For stationary measurements, the control, evaluation, and display unit can be realized by a PC. In mobile applications, a battery-powered single-board computer (SBC, Raspberry Pi 3, Raspberry Pi Foundation, Cambridge, U.K.) is used.

To measure two bioimpedances with the same hardware, the principle of time multiplexing is used. The BioZ-AFE generates the multifrequency excitation currents and applies them alternately to the electrodes of the two channels. The resulting voltages are also derived from the BioZ-AFE and analog preprocessed. Subsequently, they are fed to the COM\_IF for further processing. In order to be able to allocate the multiplexing in time afterward, an additional synchronization signal (SYNC) is sent to the COM\_IF. The COM\_IF digitizes the measurement signals and sends them together with the corresponding SYNC data via Ethernet to the computer. In addition, the interface can be used to control the analog amplifiers of the BioZ-AFE. To comply with the electrical safety requirements, the Ethernet interface is electrically isolated with a medical Ethernet isolator and the measurement system is powered either by a battery or by a medical power supply. A Python (version 3.9) script operates on the SBC or PC, which transforms the acquired signals into 25 complex impedance spectra per second and per channel in real-time. In addition, it plots and saves the data.

3) *Bioimpedance Analog Front End*: In order to be capable of generating arbitrary waveforms for current excitation, a microcontroller (ATSAM4S2BA, Microchip Technology Inc., Chandler, AZ, USA) with integrated digital-to-analog converter (DAC,  $f_s = 1$  MHz, 12 bits) is implemented on the analog front-end (AFE). For multifrequency measurement, this synthesizes a mixed signal  $S_{DAC}$ , which is composed of several harmonic signals with different frequencies. Since the DAC can only generate positive voltages, half of the maximum output voltage (FullScale) is added as an additional direct current (dc) component as shown in (1). This results in a time signal as illustrated in Fig. 5

$$S_{DAC} = \frac{\text{FullScale}}{2} + \sum_{i=1}^8 \sin(2\pi f_i t)$$

$$f = \{20, 50, 80, 110, 140, 170, 200, 230\} \text{ kHz. (1)}$$

In addition, the microcontroller controls the multiplexers MUX<sub>C</sub> and MUX<sub>V</sub> (MAX4523, Analog Devices Inc., Norwood, MA, USA) to switch between the analyzed bioimpedances  $Z_1$  and  $Z_2$ . To remove the harmonics, the signal generated by the DAC is first band-limited by the active low-pass filter LP\_C1 ( $N = 4$ ,  $f_c = 400$  kHz), realized with operational amplifiers (OPAMP, LMH6646, Dallas, TX, USA). Subsequently, the dc component is removed by the passive high-pass filter HP\_C1 ( $N = 1$ ,  $f_c = 200$  Hz). The OPAMP-based (AD8130, Analog Devices Inc.) voltage-controlled current source (VCCS) converts the voltage into a corresponding current. The corresponding electronic circuit

has already been published [45]. Depending on the multiplexer position, this current flows through  $Z_1$  or  $Z_2$  and then through the shunt resistor  $R_S$ . The resulting voltage across the bioimpedance chosen via the multiplexer MUX<sub>V</sub> (MAX4523, Analog Devices Inc.) and the voltage across  $R_S$  are processed simultaneously in identical analog signal processing chains. First, the differential signals are amplified with a programmable gain amplifier (PGA\_C1, PGA\_V1, AD8250, Analog Devices Inc.) and converted into signals with ground reference. The following passive high-pass filters (HP\_C2, HP\_V,  $N = 1$ ,  $f_c = 1$  kHz) remove the dc components and low-frequency disturbances. Then, the signals are each amplified by a second PGA (PGA\_C2, PGA\_V2, AD8250, Analog Devices Inc.) Since the ADCs can also only process positive voltage signals, operational amplifier circuits (OPA2134, Texas Instruments) are used to add half the operating voltage to the alternating signals before digitization.

The photograph in Fig. 6 shows the developed and manufactured circuit board of the AFE. It has dimensions of  $87 \times 54$  mm, which approximately correspond to those of a credit card.

### III. RESULTS AND DISCUSSION

#### A. System Characteristics

1) *Excitation Signal Generation*: Before characterizing the actual impedance measurement, the generation of the excitation current is analyzed. For this, a  $100 \Omega$  resistor with a tolerance of 0.1% was connected to the measurement terminals and the resulting voltage drop was recorded with an oscilloscope (Teledyne LeCroy HDO4054, 12 bit,  $f_s = 100$  MHz). The resulting signal is shown in the time and frequency domain in Fig. 7.

The shape of the signal corresponds to that of the simulated one in Fig. 5, but the high-frequency converting artifacts have been reduced by the reconstruction filters. There are also no more undesired signal frequencies in the spectrum visible. The effective current is approximately  $330 \mu\text{A}$  and thus fulfills the requirements of the standard for medical electrical equipment (IEC 60601-1).

2) *Systematic Errors*: The systematic errors are not relevant in many applications. For example, for muscle contraction detection or arterial pulse wave detection relative impedance changes are analyzed. However, in some applications, such as body composition measurement, the absolute values of bioimpedance are required. In addition, absolute values can be helpful in deciding if measurement results are plausible and in detecting connection problems. In order to determine the systematic errors of the measurement system, 15 known resistances  $\{12; 15; 18; 22; 27; 33; 39; 47; 56; 68; 82; 100; 120; 150; 180\} \Omega$  with tolerances of 0.1% were measured for a duration of 30 s. Afterward, the resulting 750 values per resistance were averaged to remove statistical errors. Due to the measurement principle and the calculation of the impedance spectra via dividing the complex voltage spectra by the current spectra, we assumed that constant phase errors as well as magnitude or frequency dependencies are covered by these measurements. The measurement results are shown in Figs. 8 and 9.

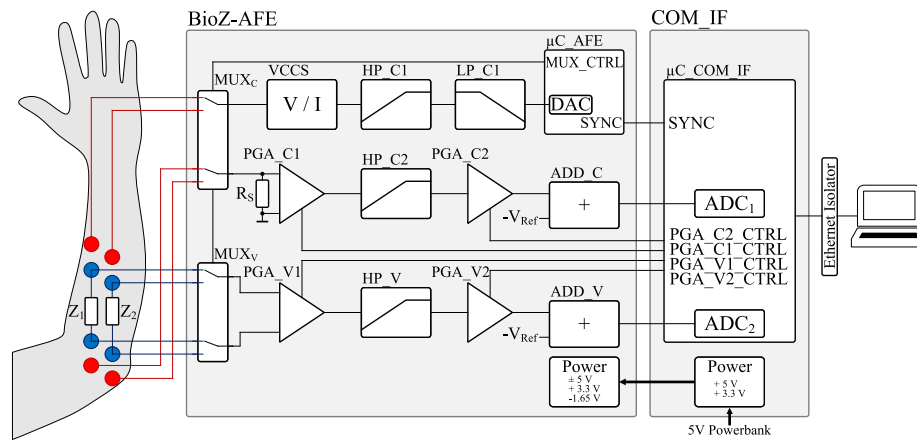


Fig. 4. Block diagram of the developed EIM measurement system, consisting of a BioZ-AFE, a COM\_IF, and a computer for analysis and display.

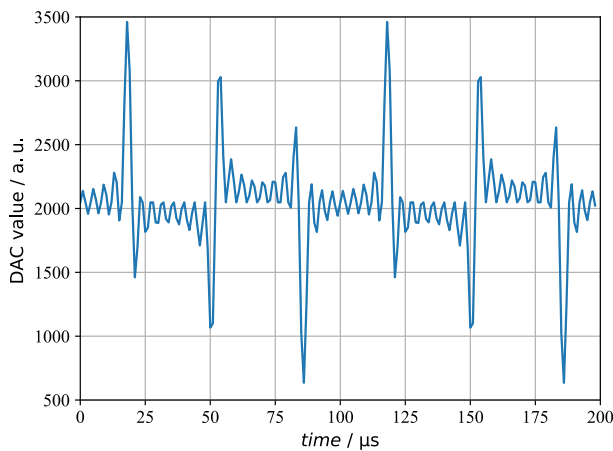


Fig. 5. Calculated function of digital values for the 12 bits DAC.

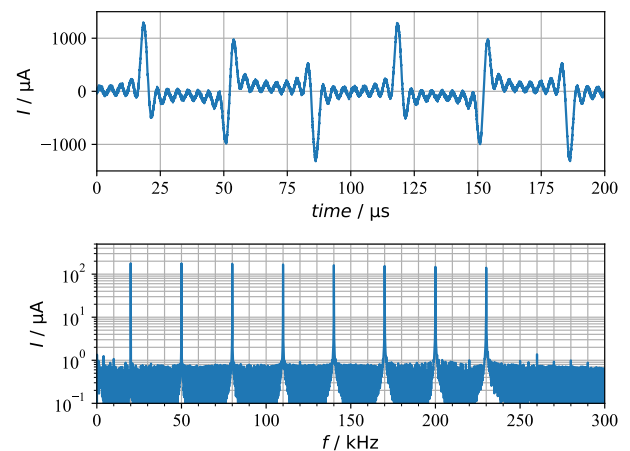


Fig. 7. Current signal across a  $100\ \Omega$  resistor measured with an oscilloscope. The root mean square (rms) value of the current is approximately  $330\ \mu\text{A}$ .

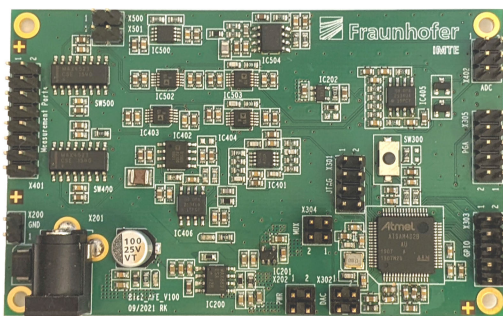


Fig. 6. Photograph of the AFE which generates the excitation current and preprocesses the measured voltages.

In Fig. 8, the relative systematic measurement errors of the impedance magnitude as a function of frequency and resistance value are plotted. It can be seen that the absolute error is lower than 1.5% in all cases. In Fig. 9, the corresponding absolute phase errors are plotted. These are always below  $1.2^\circ$  and depend on the resistance and the frequency. Especially low resistances and high measuring frequencies result in higher errors than expected. However, the requirements of Section II-B.1 are met for both magnitude measurement and phase measurement.

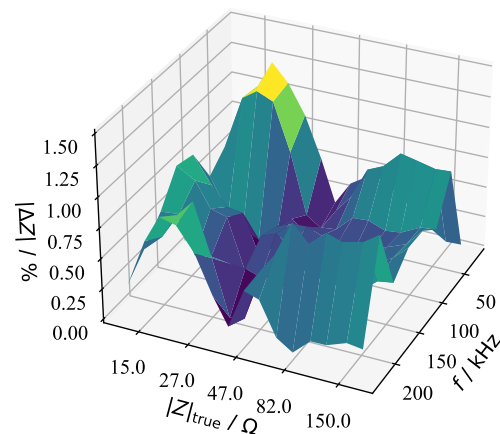
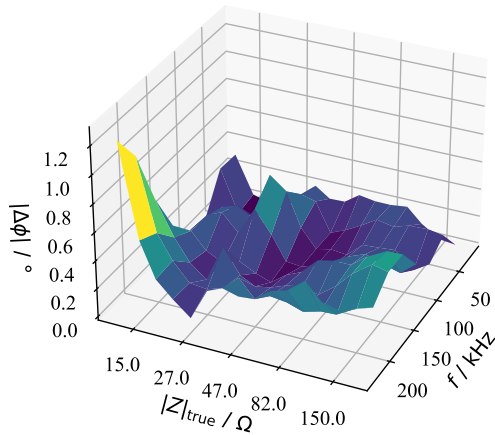
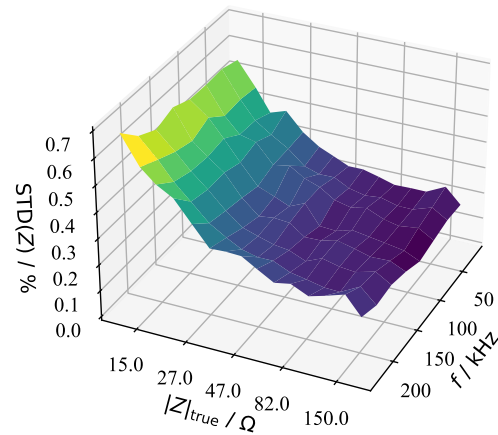


Fig. 8. Systematic errors of the bioimpedance measurement system depending on impedance and frequency. The relative measurement errors of the impedance magnitude are shown.

3) *Statistical Errors*: The statistical errors are crucial for the use of the measurement system for the detection of temporal tissue changes as they occur in EIM. To characterize these, the 15 known resistances have been measured for a duration



**Fig. 9.** Systematic errors of the bioimpedance measurement system depending on impedance and frequency. The absolute phase errors are plotted.



**Fig. 11.** Statistical errors of the bioimpedance measurement system depending on impedance and frequency. The relative STDs of the impedance magnitude measurements are shown.

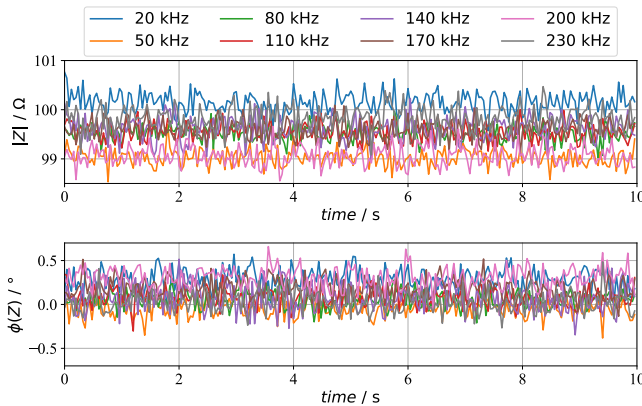


**Fig. 10.** Exemplary measurement of a 100  $\Omega$  resistor for a duration of 10 s with eight measuring frequencies from 20 to 230 kHz.

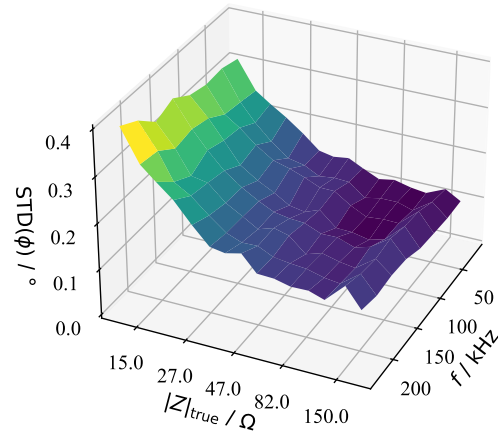


**Fig. 12.** Statistical errors of the bioimpedance measurement system depending on impedance and frequency. The STDs of the phase measurements are plotted.

of 30 s each. As an example, the raw data recorded from a 100  $\Omega$  resistance is plotted in Fig. 10.

For a better representation of the frequency and magnitude influence on the statistical errors, the standard deviation (STD) results are shown in Figs. 11 and 12. In Fig. 11, it can be seen that the relative statistical magnitude errors are below 1% in all configurations. As expected, the relative error values increase with lower resistance values or with increasing frequencies. Fig. 12 shows the STD values for the statistical phase errors. These are always below 0.4 $^\circ$  and have similar behavior in terms of dependency on the frequency and impedance magnitude. Both the statistical errors of the magnitude measurement and the phase measurement meet the requirements and are thus sufficiently low to perform an EIM with the developed system.

**4) Long-Term Drift:** The impedance changes over time do not always occur as quickly as with EIM or arterial pulse wave detection. In some cases of impedance spectroscopy, significantly slower processes are also observed. This could be, for example, the filling and emptying of the bladder. In order to estimate the errors caused by drift effects, a 100  $\Omega$  resistance was measured for a period of 30 min, corresponding to 45 000 complex impedance frequency responses. To minimize the

influence of the previously analyzed statistical errors, the results were smoothed with a moving average with a duration of 40 s. The drift effects for the magnitude ranged from 329 to 566 ppm depending on the frequency. For the phase, the errors due to drift effects are between 0.016 $^\circ$  and 0.027 $^\circ$  depending on the frequency.

**5) Step Response:** Despite the complexity of the signal acquisition, it must be ensured that both measuring channels do not have a time offset that would lead to erroneous measurement results. In addition, the signal processing methods used, such as the analog filters, must not oscillate to such an extent that they influence the signal shape. To check the dynamic system behavior, the step response of both impedance measurement channels was therefore recorded. For this purpose, a 100  $\Omega$  resistor was measured by both channels simultaneously. During the measurement, this resistor was short-circuited for a duration of approx. 450 ms. The measured signal is shown in Fig. 13. For better visualization, only the plots for 50 kHz are shown. It can be seen how the measured impedances suddenly decrease from 100 to 0  $\Omega$  and then increase again to 100  $\Omega$ . Both impedance measurements are directly on top of each other, which means that the synchronicity of the channels is ensured, and due to the multiplexing, the maximum shift is

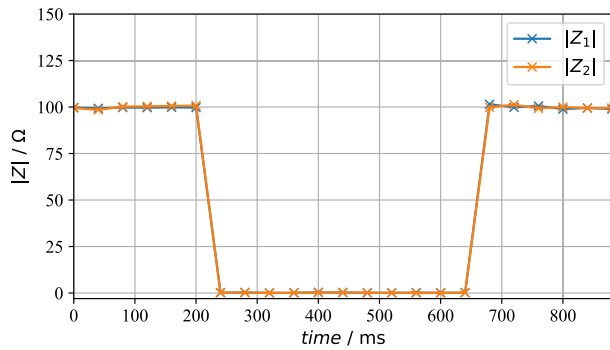


Fig. 13. Step responses of both impedance measurement channels. For better visualization, only the 50 kHz plots of the magnitudes are shown.

one sample. Neither after the decrease nor after the increase of the impedance are significant oscillations visible in the signals. This ensures that all changes in measurements are due to actual impedance variations and not to circuit influences.

6) *Electrode-Skin Impedances*: Measurements under real conditions are also affected by the electrode-skin interfaces, especially by the corresponding electrode-skin impedances  $Z_{ESI}$ . Depending on the contact material, the skin conditions and the accumulation of fluids under the electrodes the electrical characteristics can vary widely. In the typical bioimpedance measurement setup, there are four electrodes which can influence the results. Since the applied current is measured for calculating the impedances, effects on the current source are not crucial. High impedances of the negative current electrode cause common voltages in the acquired differential signal. Since differential amplifiers typically have a high common-mode rejection, this influence is also small. More relevant are the combinations of voltage electrodes and input impedances of the PGAs. In particular, the complex voltage dividers, consisting of  $Z_{ESI}$  and common mode input impedances. If these voltage dividers are imbalanced, the corresponding part of the common-mode voltage at this point becomes a differential voltage. Since this is applied directly to the amplifier input it is amplified accordingly. At low frequencies, the resistive part of the input impedances is dominant. This is over 1 G $\Omega$  and therefore significantly higher than typical electrode-skin impedances [46]. However, due to the capacitive properties of the input impedances, these become low at high frequencies. In the system presented here, the combination of multiplexer and PGA results in input capacities of 7 pF. At the highest measuring frequency of 230 kHz, this results in input impedances of only approximately 100 k $\Omega$ . In the particular measurement application, it must therefore be ensured that either both voltage electrodes have the same contact impedance or that the contact impedances are much lower than the system's input impedances. In practice, the first is hardly feasible. However, preliminary work has shown that gel electrodes in particular have sufficiently low and stable contact impedances and that their influence on the measurement is therefore low [46].

## B. Measurements

1) *Phantom Measurements*: Before performing measurements on human tissue, it is ensured that the system is capable

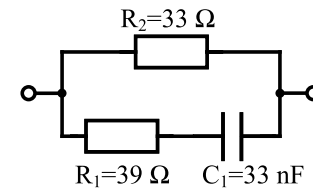


Fig. 14. Electrical phantom to simulate the electrical behavior of tissue.

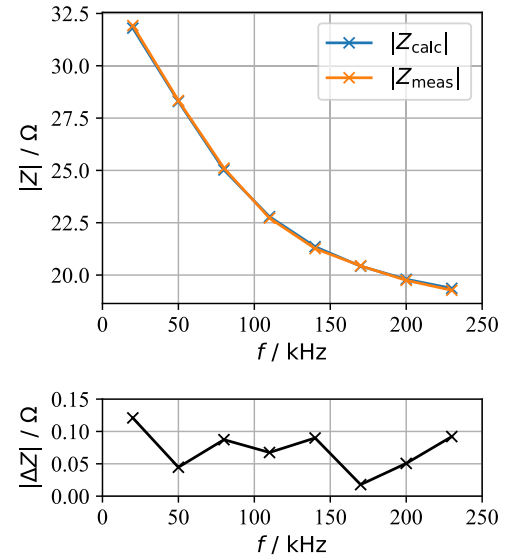


Fig. 15. Calculated (blue) and measured (orange) magnitude response of the electrical tissue phantom. At the top, the plots of the magnitude response are shown. Below, the absolute difference is plotted.

of measuring complex impedances with a capacitive component. For this, the electrical RCR model from Fig. 1(b) is used. In order to reproduce the characteristic electrical behavior of the bioimpedance magnitude and phase over frequency, the realistic values  $R_1 = 39 \Omega$ ,  $R_2 = 33 \Omega$  and  $C_1 = 33 \text{ nF}$  are chosen, as shown in Fig. 14 [21], [47].

Components with uncertainties of 0.1% are used to realize the phantom.

The phantom was measured with the developed system for a duration of 10 s, corresponding to 250 samples. The resulting averaged magnitude response is shown in Fig. 15 and the corresponding phase response in Fig. 16. In the upper plots, the measured (orange) and the simulated curves (blue) calculated with ideal component values are shown for comparison. The absolute differences are shown below each figure. These are within the range of systematic measurement errors investigated in Section III-A.2. This shows that the measurement system can also reliably measure complex impedances.

2) *Subject Measurements on Antagonistic Forearm Muscles*: Many parts of the human musculoskeletal system work antagonistically. The contracting muscle is called agonist and the corresponding relaxing muscle is called antagonist. While EMG can only detect contractions, bioimpedance measurements can also be used to detect the changing geometric tissue properties of the relaxed muscles. Since the antagonistic muscle pairs move inversely to each other during

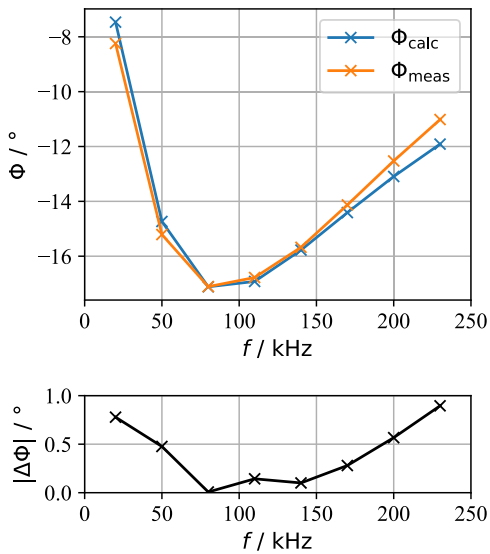


Fig. 16. Calculated (blue) and measured (orange) phase response of the electrical tissue phantom. At the top, the plots of the phase response are shown. Below, the absolute difference is plotted.

concentric contractions, this behavior is also to be expected from the bioimpedance. For safety-critical applications, such as the control of prostheses, the two independent sources of information can be used to increase the robustness of the control. For the exemplary measurement of antagonistic muscles, the forearm was chosen. The study was conducted in accordance with the Declaration of Helsinki, and approved by the Institutional Ethics Committee of the University of Lübeck (#21-020, February 16, 2022). As shown in the photograph in Fig. 17, four electrodes each are placed on the upper side of the forearm and the underside of the forearm to measure the bioimpedances. The electrodes of channel 1 (CH1) are located above the extensor carpi radialis longus and the electrodes of channel 2 (CH2) are located above the flexor carpi radialis. The electrodes for applying the excitation currents to the tissue are located on the outside and the two inner electrodes are used for voltage measurements. To ensure good and stable contacting conditions gel electrodes with the dimensions of  $45 \times 22 \text{ mm}$  and a contact area of  $95 \text{ mm}^2$  are used (Ambu BlueSensor N). To avoid mechanical coupling between the electrodes, there is a clearance of approximately 2 mm between the current and voltage electrodes. The distances between the contact surfaces of the voltage electrodes are approx. 10–20 mm, resulting in a definite longitudinal measurement direction and at the same time limiting the measurement geometrically to the muscle region to be analyzed.

During the bioimpedance measurement, typical hand movements were performed. As shown in Fig. 18, these were the wrist extension (WE) and the wrist flexion (WF). The subject was asked to first hold the hand in the middle position. Then the subject started with a WE for approximately 3 s and moved the hand back to the middle position. Subsequently, a WF was performed for a duration of about 3 s and again the hand was moved to mid-position. This sequence was repeated several times.

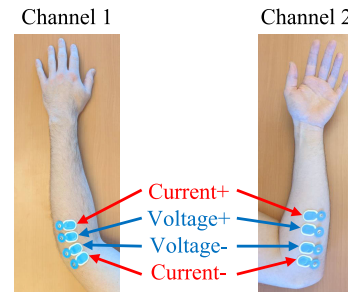


Fig. 17. Electrodes placement of both impedance measurement channels to acquire the bioimpedances of antagonistic forearm muscles.

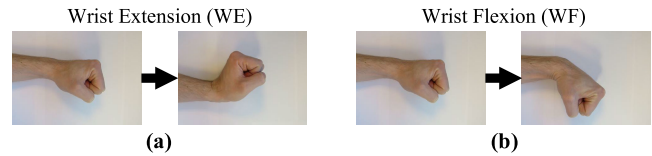


Fig. 18. Performed movements to contract the antagonistic muscle groups were (a) WE and (b) WF.

The measurement results are shown for the duration of 30 s in Fig. 19. To reduce the influence of statistical measurement errors, all signals were smoothed by a moving average filter ( $N = 10$ ). The upper two plots show the changes in the bioimpedance magnitudes of CH1 and CH2 during the movements. It can be clearly seen that for all measurement frequencies the impedance magnitude  $|Z_1|$  of CH1 is reduced during WE and slightly increased during WF. As expected, the behavior of  $|Z_2|$  is the opposite. For instance, WE leads to increases in impedance magnitude and WF leads to decreases. The phase plots below look similar but differ in one important aspect. It can be seen that the WE periods cause the phases to become more positive in the  $\phi(Z_1)$  plots for almost all chosen measurement frequencies. However, for particularly low frequencies, e.g., 20 kHz, the phase becomes more negative. A similar behavior can be seen in the  $\phi(Z_2)$  plots. The phase curves of low and high frequencies behave opposite to each other. As described in Section II-A, this particular phase behavior was expected and represents a feature in the EIM that can be used to detect muscle contractions with high reliability. Especially in the  $\phi(Z_2)$  plots it can be seen that also contractions of different muscles can be clearly distinguished from each other.

For a more detailed analysis of the two selected movements WE and WF and the resulting impedance changes, further measurements are performed. For this purpose, the subject was asked to perform several WE or WF in succession. The measurement results were also smoothed with a moving average filter ( $N = 10$ ). Fig. 20 shows the results for the WE for a duration of 6 s. Again, it can be seen that during the contractions  $|Z|$  decreases for all frequencies of CH1 and increases accordingly for CH2. The maximum absolute magnitude changes occur at low measurement frequencies. For example, for  $f = 20 \text{ kHz}$ , a WE causes a decrease of  $|Z_1|$  from 70.5 to 67  $\Omega$ , which is approximately 5%. At higher measurement frequencies, the absolute magnitude changes are

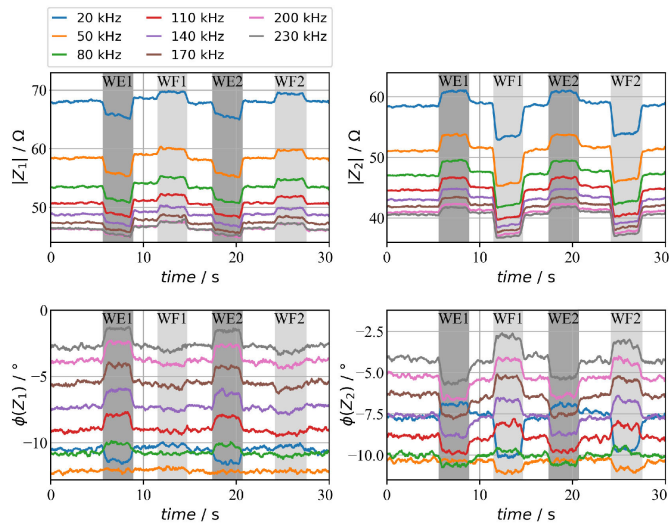


Fig. 19. Measured bioimpedance magnitudes and phases of both channels for eight chosen frequencies during WE and WF movements. The movements were separated by moving the hand into the middle position.

smaller, but are also about 5% in relative terms. Although the corresponding changes in  $|Z_2|$  are similar in magnitude in this example, as can be seen in the previous measurement, the values of the agonist muscles can also be significantly different from those of the antagonist muscles. No general statement can be made for the influence of muscle contraction on the phase, instead the measurement frequencies must be taken into account. As described above, the phase of CH1 becomes more positive during WE muscle contraction for high frequencies and more negative at low frequencies. For the measurement frequency in-between of  $f = 50$  kHz, the contraction has almost no effect on the phase. An inverse behavior can be seen for  $\phi(Z_2)$ .

The lower plots show the frequency responses of  $Z_1$  and  $Z_2$  during relaxation and contraction. For this, time periods of 0.8 s each, which corresponds to 20 samples, were averaged. Here it can be clearly seen that  $|Z_1|$  decreases by approximately 5% during contraction and  $|Z_2|$  increases by about 5%, regardless of the measurement frequency. In the phase responses, the absolute phase change increases with distance from the intersection point at about 50 kHz. Measuring frequencies significantly below 50 kHz and above are therefore desirable. However, low measurement frequencies are limited due to electrical safety, and significantly higher frequencies are associated with more complex measurement technology.

This measurement was repeated for the WF motion. The filtered signals are shown in Fig. 21. As expected, during contraction the impedance magnitudes  $|Z_1|$  of CH1 increase, because in this situation they represent the antagonistic muscles.  $Z_2$ , on the other hand, is acquired at the underside of the forearm and thus represents the impedance behavior of the contracting muscles. Accordingly, during the flexion the magnitudes  $|Z_2|$  decrease. The phase changes  $\phi(Z_1)$  in CH1 over time are too small in this measurement to reliably distinguish them from the statistical measurement errors. The

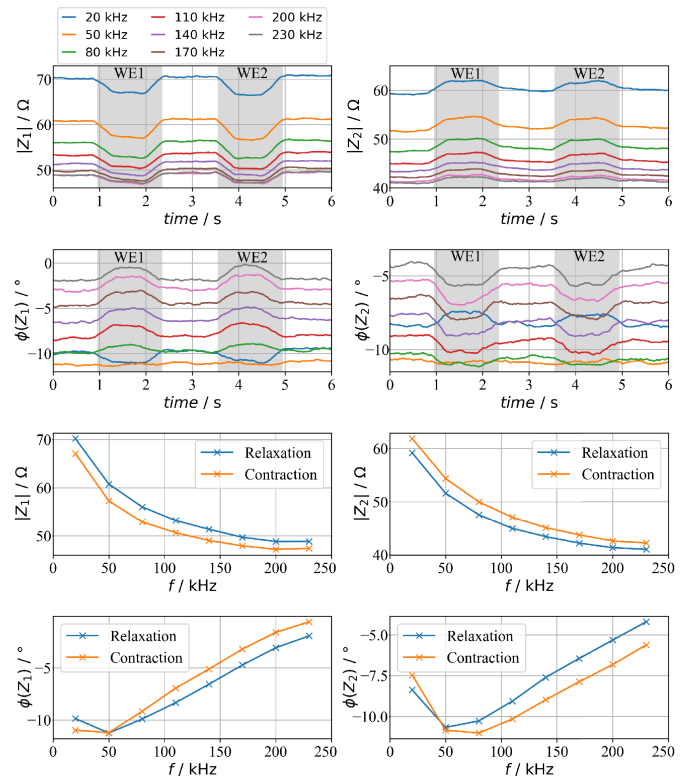


Fig. 20. Measured bioimpedances during WEs. The upper plots show the timing behavior and the lower plots represent the frequency responses during relaxation and contraction.

phase plots  $\phi(Z_2)$  of CH2 are more useful and the particular frequency dependency of the phase is visible.

In the frequency responses of CH1 the small changes of the magnitude  $|Z_1|$  between the relaxation and contraction can be seen. Also in this representation, the changes in  $\phi(Z_1)$  are too small for reliable detection. However, the frequency response of CH2 contains more information. The significant magnitude changes and phase changes are clearly visible and, as expected, are inverse to those from the previous plot in Fig. 20.

The measurements demonstrate that the system is capable of detecting the relationships between agonistic and antagonistic muscles. It could also be shown that the effects occurring in the bioimpedances are complex, especially in the phase responses. More extensive subject measurements and signal evaluations are needed to also identify the temporal relationships of antagonistic muscle pairs.

3) *Directional Dependence of the EIM*: In the past, the frequency responses of bioimpedance during a muscle contraction were analyzed exclusively in the fiber direction. Simultaneous measurement of bioimpedance in orthogonal direction was not possible so far, therefore there is no reliable knowledge regarding directional dependence. The presented dual-channel measurement system enables such measurements. For exemplary application, an EIM is again performed on the forearm using the same gel electrodes. But, as shown in Fig. 22, this measurement uses both channels to measure the same tissue area. For this purpose, the four electrodes of each of the two channels are positioned on the underside of the forearm above the flexor carpi radialis. However, the

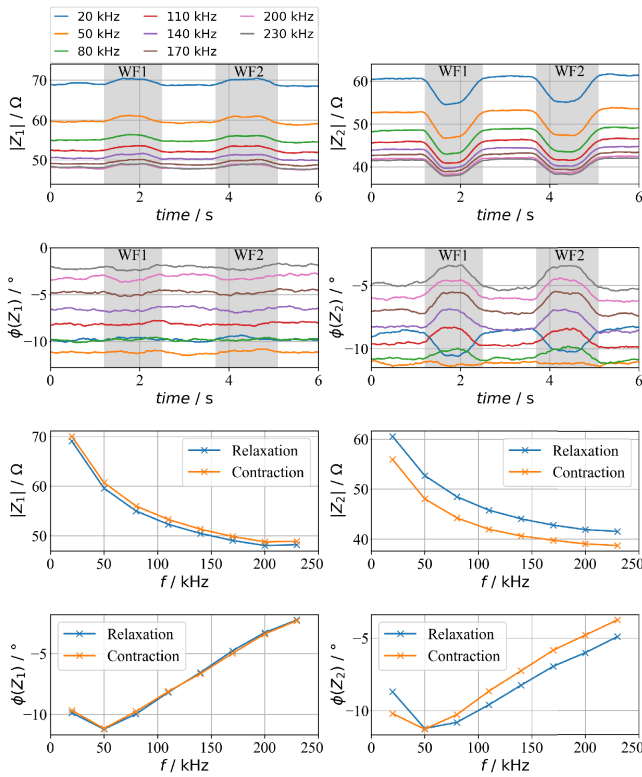


Fig. 21. Measured bioimpedances during WFs. The upper plots show the timing behavior and the lower plots represent the frequency responses during relaxation and contraction.

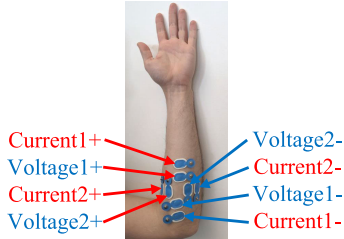


Fig. 22. Electrodes placement to measure simultaneously the bioimpedance in two orthogonal directions for analyzing the directional dependence.

electrode alignment and thus the impedance measurements are orthogonal to each other. The subject is asked to perform several WF movements during this measurement.

The resulting impedance signals for the duration of 8 s are shown in Fig. 23.

As in the results shown above, the muscle contractions cause significant decreases in bioimpedance along the muscle fiber, corresponding to  $|Z_1|$  in this measurement. The behavior of the phase signals  $\phi(Z_1)$  and the plot of  $Z_1$  in the frequency domain are also similar to the previous results. A comparison of the four plots of  $Z_1$  with the respective plots for  $Z_2$  shows that both magnitude and phase are almost identical during the muscle contractions. Only the absolute values are slightly different, which is reasonable due to the tissue anisotropy of muscles. If these results are confirmed by further subject measurements, this would be a great advantage for the placement of the measuring electrodes. These would no longer need to

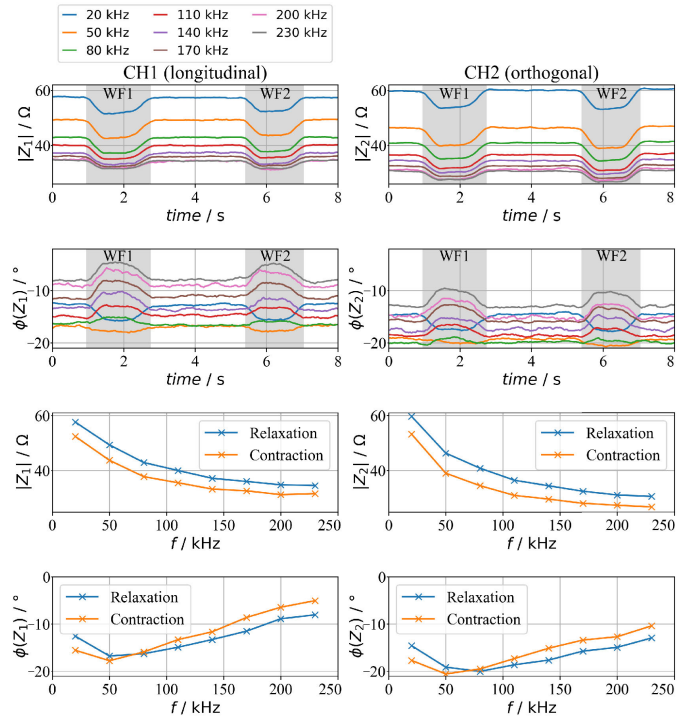


Fig. 23. Measurement result of the orthogonally measured bioimpedances during WFs.

be manually oriented for the purpose of muscle contraction detection using bioimpedance analysis. In addition, special electrode shapes such as ring electrodes could be implemented.

#### IV. CONCLUSION

The acquisition of the complex bioimpedance as a function of frequency has been known for a long time, but still has much potential when the instrumentation is extended. The goals of this work were in particular the dual-channel measurement and real-time capability for detection of muscle contractions. For this purpose, a portable measuring system was developed and characterized metrologically. After the functionality was verified using an electrical phantom, the first subject measurements were performed. These have demonstrated that the system can also measure real tissue and is capable of detecting muscle contractions. The system was used for the first time to simultaneously measure and compare the complex frequency responses of two antagonistic muscles during contraction. The usefulness of multifrequency measurement, especially that of the phase response and also that of dual-channel measurements for reliable detection of muscle contractions, could be demonstrated. In a further pilot measurement, the directional dependence of impedance changes during muscle contraction was investigated. The first results indicate that this dependence is very low. While the anisotropy of tissue structures certainly affects the values of the bioimpedance, the temporal effects of impedance during muscle contraction in the fiber direction are similar to these in orthogonal direction. The measurements have been primarily used to check the functionality of the measurement system. However, new ideas for measurement approaches also emanate from them. In order to make reliable statements

in the future, extensive studies on many subjects and under varying measurement conditions will be required. In addition, simultaneous acquisition of the corresponding EMG signals would be helpful for analysis.

## REFERENCES

- [1] K. R. Wheeler, M. H. Chang, and K. H. Knuth, "Gesture-based control and EMG decomposition," *IEEE Trans. Syst., Man Cybern., C, Appl. Rev.*, vol. 36, no. 4, pp. 503–514, Jul. 2006.
- [2] S. Bitzer and P. van der Smagt, "Learning EMG control of a robotic hand: Towards active prostheses," in *Proc. IEEE Int. Conf. Robot. Autom. (ICRA)*, May 2006, pp. 2819–2823.
- [3] K. Kiguchi, T. Tanaka, and T. Fukuda, "Neuro-fuzzy control of a robotic exoskeleton with EMG signals," *IEEE Trans. Fuzzy Syst.*, vol. 12, no. 4, pp. 481–490, Aug. 2004.
- [4] J. Qi, G. Jiang, G. Li, Y. Sun, and B. Tao, "Intelligent human–computer interaction based on surface EMG gesture recognition," *IEEE Access*, vol. 7, pp. 61378–61387, 2019.
- [5] C. J. De Luca, A. Adam, R. Wotiz, L. D. Gilmore, and S. H. Nawab, "Decomposition of surface EMG signals," *J. Neurophysiol.*, vol. 96, no. 3, pp. 1646–1657, Sep. 2006.
- [6] M. Zahak, "Signal acquisition using surface EMG and circuit design considerations for robotic prosthesis," in *Computational Intelligence in Electromyography Analysis—A Perspective on Current Applications and Future Challenges*. London, U.K.: InTech, Oct. 2012.
- [7] R. N. Khushaba, S. Kodagoda, M. Takruri, and G. Dissanayake, "Toward improved control of prosthetic fingers using surface electromyogram (EMG) signals," *Expert Syst. Appl.*, vol. 39, no. 12, pp. 10731–10738, Sep. 2012.
- [8] A. Prakash, S. Sharma, and N. Sharma, "A compact-sized surface EMG sensor for myoelectric hand prosthesis," *Biomed. Eng. Lett.*, vol. 9, no. 4, pp. 467–479, Nov. 2019.
- [9] M. M. Shobaki et al., "High quality acquisition of surface electromyography—Conditioning circuit design," *IOP Conf. Ser., Mater. Sci. Eng.*, vol. 53, Dec. 2013, Art. no. 012027.
- [10] M.-S. Song, S.-G. Kang, K.-T. Lee, and J. Kim, "Wireless, skin-mountable EMG sensor for human–machine interface application," *Micromachines*, vol. 10, no. 12, p. 879, Dec. 2019.
- [11] Y.-D. Wu, S.-J. Ruan, and Y.-H. Lee, "An ultra-low power surface EMG sensor for wearable biometric and medical applications," *Biosensors*, vol. 11, no. 11, p. 411, Oct. 2021.
- [12] I. Mazzetta et al., "Stand-alone wearable system for ubiquitous real-time monitoring of muscle activation potentials," *Sensors*, vol. 18, no. 6, p. 1748, May 2018. [Online]. Available: <https://www.mdpi.com/1424-8220/18/6/1748>
- [13] A. Phinyomark and E. Scheme, "EMG pattern recognition in the era of big data and deep learning," *Big Data Cognit. Comput.*, vol. 2, no. 3, p. 21, Aug. 2018.
- [14] R. Chowdhury, M. Reaz, M. Ali, A. Bakar, K. Chellappan, and T. Chang, "Surface electromyography signal processing and classification techniques," *Sensors*, vol. 13, no. 9, pp. 12431–12466, Sep. 2013.
- [15] B. R. Schlink, A. D. Nordin, and D. P. Ferris, "Comparison of signal processing methods for reducing motion artifacts in high-density electromyography during human locomotion," *IEEE Open J. Eng. Med. Biol.*, vol. 1, pp. 156–165, 2020.
- [16] S. B. Rutkove, "Electrical impedance myography: Background, current state, and future directions," *Muscle Nerve*, vol. 40, no. 6, pp. 936–946, Dec. 2009.
- [17] G. Hornero, D. Díaz, and O. Casas, "Bioimpedance system for monitoring muscle and cardiovascular activity in the stump of lower-limb amputees," *Physiol. Meas.*, vol. 34, no. 2, pp. 189–201, Jan. 2013.
- [18] R. Kusche and M. Ryschka, "Combining bioimpedance and EMG measurements for reliable muscle contraction detection," *IEEE Sensors J.*, vol. 19, no. 23, pp. 11687–11696, Dec. 2019.
- [19] C. Ngo et al., "A wearable, multi-frequency device to measure muscle activity combining simultaneous electromyography and electrical impedance myography," *Sensors*, vol. 22, no. 5, p. 1941, Mar. 2022.
- [20] Y. Cho, P. Kim, and K.-S. Kim, "Electrical impedance myography (EIM) for multi-class prosthetic robot hand control," in *Proc. 20th Int. Conf. Control, Autom. Syst. (ICCAS)*, Oct. 2020, pp. 1092–1094.
- [21] R. Kusche and M. Ryschka, "Multi-frequency impedance myography: The PhaseX effect," *IEEE Sensors J.*, vol. 21, no. 3, pp. 3791–3798, Feb. 2021.
- [22] O. G. Martinsen and S. Grimnes, *Bioimpedance and Bioelectricity Basics*. New York, NY, USA: Academic, Aug. 2014.
- [23] G. J. Saulnier et al., "An electrical impedance spectroscopy system for breast cancer detection," in *Proc. 29th Annu. Int. Conf. IEEE Eng. Med. Biol. Soc.*, Aug. 2007, pp. 4154–4157.
- [24] S. Kaufmann, A. Malhotra, G. Ardelt, and M. Ryschka, "A high accuracy broadband measurement system for time resolved complex bioimpedance measurements," *Physiol. Meas.*, vol. 35, no. 6, pp. 1163–1180, May 2014.
- [25] F. Campa, S. Toselli, M. Mazzilli, L. A. Gobbo, and G. Coratella, "Assessment of body composition in athletes: A narrative review of available methods with special reference to quantitative and qualitative bioimpedance analysis," *Nutrients*, vol. 13, no. 5, p. 1620, May 2021.
- [26] J. Ferreira, I. Pau, K. Lindecrantz, and F. Seoane, "A handheld and textile-enabled bioimpedance system for ubiquitous body composition analysis. An initial functional validation," *IEEE J. Biomed. Health Informat.*, vol. 21, no. 5, pp. 1224–1232, Sep. 2017.
- [27] R. Kusche, P. Klimach, and M. Ryschka, "A multichannel real-time bioimpedance measurement device for pulse wave analysis," *IEEE Trans. Biomed. Circuits Syst.*, vol. 12, no. 3, pp. 614–622, Jun. 2018.
- [28] M. R. Scudder et al., "Dual impedance cardiography: An inexpensive and reliable method to assess arterial stiffness," *Psychophysiology*, vol. 58, no. 7, pp. 1–14, Jan. 2021.
- [29] S. Chabchoub, S. Mansouri, and R. Ben Salah, "Detection of valvular heart diseases using impedance cardiography ICG," *Biocybern. Biomed. Eng.*, vol. 38, no. 2, pp. 251–261, 2018.
- [30] R. Kusche, A.-V. Lindenberg, S. Hauschild, and M. Ryschka, "Aortic frequency response determination via bioimpedance plethysmography," *IEEE Trans. Biomed. Eng.*, vol. 66, no. 11, pp. 3238–3246, Nov. 2019.
- [31] A. Koblelev, A. Briko, V. Popova, V. Kapravchuk, S. Shchukin, and A. Saltykova, "Determination of the muscle longitudinal electrical resistivity in-vivo during contraction," in *Proc. Ural-Siberian Conf. Biomed. Eng., Radioelectronics Inf. Technol. (USBREIT)*, Sep. 2022, pp. 70–73.
- [32] T. R. Farrell and R. F. Weir, "The optimal controller delay for myoelectric prostheses," *IEEE Trans. Neural Syst. Rehabil. Eng.*, vol. 15, no. 1, pp. 111–118, Mar. 2007.
- [33] K. Dheman, P. Mayer, M. Eggimann, S. Schuerle, and M. Magno, "ImpediSense: A long lasting wireless wearable bio-impedance sensor node," *Sustain. Comput., Informat. Syst.*, vol. 30, Jun. 2021, Art. no. 100556.
- [34] M. Usman, A. K. Gupta, and W. Xue, "Wearable ring bioelectrical impedance analyzer for estimation and monitoring of body fat," *Smart Health*, vol. 24, Jun. 2022, Art. no. 100275.
- [35] C. Qiu, F. Wu, W. Han, and M. R. Yuce, "A wearable bioimpedance chest patch for real-time ambulatory respiratory monitoring," *IEEE Trans. Biomed. Eng.*, vol. 69, no. 9, pp. 2970–2981, Sep. 2022.
- [36] S. Critcher and T. J. Freeborn, "System performance and user feedback regarding wearable bioimpedance system for multi-site knee tissue monitoring: Free-living pilot study with healthy adults," *Frontiers Electron.*, vol. 3, pp. 1–17, Apr. 2022, Art. no. 324981.
- [37] S. Mabrouk et al., "Robust longitudinal ankle edema assessment using wearable bioimpedance spectroscopy," *IEEE Trans. Biomed. Eng.*, vol. 67, no. 4, pp. 1019–1029, Apr. 2020.
- [38] M. H. Jung et al., "Wrist-wearable bioelectrical impedance analyzer with miniature electrodes for daily obesity management," *Sci. Rep.*, vol. 11, no. 1, pp. 1–10, Jan. 2021, Art. no. 1238.
- [39] A. G. Gheorghie, F. Constantinescu, M. Nițescu, and M. E. Marin, "Circuit models of bioelectric impedance," in *Electrochemical Impedance Spectroscopy*. London, U.K.: IntechOpen, Dec. 2020.
- [40] M. Yashiro and H. Kotera, "Novel equations for bioimpedance spectroscopy to calculate body fluid volume based on the agreement between body weight and extracellular water change before and after hemodialysis as a guide," *Renal Replacement Therapy*, vol. 5, no. 1, pp. 1–11, Feb. 2019, Art. no. 7.
- [41] H. C. Lukaski, "Evolution of bioimpedance: A circuitous journey from estimation of physiological function to assessment of body composition and a return to clinical research," *Eur. J. Clin. Nutrition*, vol. 67, no. 1, pp. 2–9, Jan. 2013.
- [42] L. Röthlingshöfer, M. Ulbrich, S. Hahne, and S. Leonhardt, "Monitoring change of body fluid during physical exercise using bioimpedance spectroscopy and finite element simulations," *J. Electr. Bioimpedance*, vol. 2, no. 1, pp. 79–85, Dec. 2011.
- [43] B. Sanchez and S. B. Rutkove, "Electrical impedance myography and its applications in neuromuscular disorders," *Neurotherapeutics*, vol. 14, no. 1, pp. 107–118, Jan. 2017.

- [44] B. Sanchez, A. Pacheck, and S. B. Rutkove, "Guidelines to electrode positioning for human and animal electrical impedance myography research," *Sci. Rep.*, vol. 6, no. 1, pp. 1–14, Sep. 2016, Art. no. 32615.
- [45] R. Kusche, S. Hauschild, and M. Ryschka, "Galvanically decoupled current source modules for multi-channel bioimpedance measurement systems," *Electronics*, vol. 6, no. 4, p. 90, Oct. 2017.
- [46] R. Kusche, S. Kaufmann, and M. Ryschka, "Dry electrodes for bioimpedance measurements—Design, characterization and comparison," *Biomed. Phys. Eng. Exp.*, vol. 5, no. 1, Nov. 2018, Art. no. 015001.
- [47] L. Nescolarde, J. Yanguas, H. Lukaski, X. Alomar, J. Rosell-Ferrer, and G. Rodas, "Localized bioimpedance to assess muscle injury," *Physiol. Meas.*, vol. 34, no. 2, pp. 237–245, Jan. 2013.



**Roman Kusche** (Member, IEEE) received the B.Sc. degree in electrical engineering from the Lübeck University of Applied Sciences, Lübeck, Germany, in 2013, the M.Sc. degree from the Hamburg University of Applied Sciences, Hamburg, Germany, in 2014, and the Dr.-Ing. (Ph.D.) degree from the University of Lübeck, Lübeck, in 2020.

From 2014 to 2019, he was the Research Group Leader with the Laboratory of Medical Electronics, Lübeck University of Applied Sciences. Afterward, he worked as a Senior Researcher with the Center of Excellence CoSA, Lübeck. From 2020 to 2023, he was the Head of the Department for Individualized Therapy, Fraunhofer Research Institution for Individualized and Cell-Based Medical Engineering IMTE, Lübeck. He has been appointed a Professor with the Hamburg University of Applied Sciences, since 2023. His research interests include the development of novel biomedical measurement methods and related medical sensors.



**Andra Oltmann** received the B.Sc. degree in medical engineering from Universität zu Lübeck, Lübeck, Germany, in 2017, and the M.Sc. degree in biomedical engineering from Leibniz Universität Hannover, Hannover, Germany, in 2020.

Since 2020, she has been with the Fraunhofer Research Institution for Individualized and Cell-Based Medical Engineering IMTE, Lübeck. Her research interests include electrophysiological modeling and simulation of human body muscles.



**Philipp Rostalski** (Member, IEEE) received the Dipl.-Ing. degree in electrical engineering, with a focus on measurement and control from the Hamburg University of Technology, Hamburg, Germany, in 2004, and the Ph.D. degree from ETH Zürich, Zürich, Switzerland, in 2009.

In 2005, he joined the Automatic Control Laboratory, ETH Zürich, where he worked on the interface of algebraic geometry, optimization, and control. His Ph.D. thesis was awarded with the ETH Medal for Outstanding Ph.D. theses. In

2009, he joined the Department of Mathematics, UC Berkeley, Berkeley, CA, USA, as a Feodor Lynen Fellow of the German Alexander von Humboldt Foundation, where he was working on problems in applied mathematics, most notably on convex algebraic geometry. From 2011 to 2015, he was a Research Engineer and the Project Manager of mechatronics applications with the Dräger Research Unit, Lübeck, Germany. He was responsible for projects in signal processing and control, with a focus on pneumatic systems and respiratory care. Since 2015, he has been the Director of the Institute for Electrical Engineering in Medicine, Universität zu Lübeck, Lübeck. Since 2020, he has been the Director with the Fraunhofer Research Institution for Individualized and Cell-Based Medical Engineering (IMTE), Lübeck.